ChemComm

ROYAL SOCIETY OF CHEMISTRY

COMMUNICATION

View Article Online
View Journal | View Issue

Cite this: *Chem. Commun.*, 2020, **56**, 10143

Received 19th June 2020,
Accepted 23rd July 2020

DOI: 10.1039/d0cc04283h

rsc.li/chemcomm

Structure-directing role of immobilized polyoxometalates in the synthesis of porphyrinic Zr-based metal–organic frameworks†

Mathis Duguet,[ab] Alex Lemarchand,[b] Youven Benseghir,[ab] Pierre Mialane,[a] Maria Gomez-Mingot,[b] Catherine Roch-Marchal,[a] Mohamed Haouas,[a] Marc Fontecave,[b] Caroline Mellot-Draznieks,*[b] Capucine Sassoye*[c] and Anne Dolbecq*[a]

We evidence the structure-directing role of the $PW_{12}O_{40}^{3-}$ polyoxometalate in porphyrinic MOF synthesis whereby it promotes the formation of the kinetic topology. Its immobilization into the MOF is successfully achieved at a high temperature yielding the kinetic MOF-525/PCN-224 phases, while prohibiting the formation of the thermodynamic MOF-545 product. A combined experimental/theoretical approach uses differential PDF and DFT calculations along with solid-state NMR to show the structural integrity of the POM and its location next to the Zr-based nodes.

Over the years, Metal–Organic Frameworks (MOFs) have been extensively studied for a variety of applications such as gas storage, drug delivery or catalysis.[1–3] In the strategic field of solar energy conversion, the use of porphyrinic Zr_6-TCCP-based MOFs constructed from $Zr_6O_4(OH)_4$ inorganic nodes and tetrakis(4-carboxyphenyl)porphyrin (TCPP) linkers for photo- or electrocatalysis purposes has attracted ever-growing interest, knowing that the porphyrin can act both as a photosensitizer and/or catalyst when metallated.[4,5] Amongst this subfamily, three topologies have attracted particular attention, namely **MOF-525**,[6] **PCN-224**[7] and **MOF-545**[6] (this last being also known as PCN-222) (Fig. 1). Due to the large size of the TCPP linker, these three Zr_6-TCCP-based MOFs exhibit sufficiently wide pores and high surface areas to allow the heterogenization of molecular catalysts to host energy conversion-related reactions, an emerging subfield.[8] We thus recently showed that the immobilization of a cobalt sandwich-type polyoxometalate (POM) in **MOF-545** leads to a noble metal-free heterogeneous photosystem with a high photocatalytic activity for water oxidation reaction, whereby **MOF-545** acts as both a photosensitizer and an heterogenization matrix.[9] POMs can also be co-immobilized with complexes in the pores of MOFs in order to boost their photocatalytic activity. Recently, we evidenced that the incorporation of the $PW_{12}O_{40}^{3-}$ (PW_{12}) Keggin-type POM inside the Cp*Rh@UiO-67 MOF increased its photocatalytic activity for the CO_2 reduction reaction (CO_2RR) when compared to that of the POM-free catalyst.[10] Amongst other MOFs,[11] **MOF-525** was shown to display significant catalytic activity for the CO_2RR. While Hod *et al.* first showed the electrocatalytic properties of **MOF-525(Fe)**,[12] Zhang *et al.* demonstrated, a year later, the photocatalytic activity for CO_2RR of its free-base, Co- and Zn-metallated forms under visible light.[13] Based on these studies, we decided to attempt the immobilization of PW_{12} inside the Fe-metallated Zr_6-TCPP-based MOFs in view of modifying their catalytic properties at a later stage. It must be recalled that the targeted synthesis of these phases is still a subject of intense research.[12–18] For example, the influence of the synthetic temperature[14] or that of the modulator[16] was explored, whereby **MOF-525** and **PCN-224** synthesized at room temperature (RT) were shown to be kinetic outcomes while **MOF-545** was identified as the thermodynamic

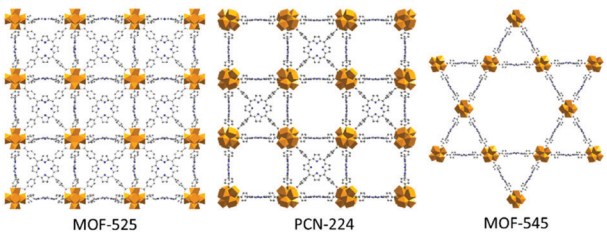

Fig. 1 The three porphyrinic Zr_6-TCCP-based MOFs encountered in this study. **MOF-525** and **PCN-224** exhibit cubic cavities, and **PCN-224** being described as a **MOF-525** with missing linkers. **MOF-545** possesses hexagonal channels.

[a] *Université Paris-Saclay, UVSQ, CNRS, UMR 8180, Institut Lavoisier de Versailles, 78035 Versailles Cedex, France. E-mail: anne.dolbecq@uvsq.fr*
[b] *Laboratoire de Chimie des Processus Biologiques, UMR CNRS 8229, Collège de France, Sorbonne Université, PSL Research University, 11 Place Marcelin Berthelot, 75231 Paris Cedex 05, France. E-mail: caroline.mellot-draznieks@college-de-france.fr*
[c] *Sorbonne Université, UMR 7574, Collège de France, Laboratoire de Chimie de la Matière Condensée de Paris, 4 Place Jussieu, 75252 Paris cedex 05, France. E-mail: capucine.sassoye@upmc.fr*

† Electronic supplementary information (ESI) available: Detailed synthesis, characterizations and computations. See DOI: 10.1039/d0cc04283h

phase obtained at a higher temperature. The consequence of the kinetic nature of **MOF-525** and **PCN-224** and of their structural similarity is that they are often obtained as a mixture, yielding very similar X-ray diffraction patterns. This led us to investigate the synthetic parameters which make it possible to get the desired kinetic Fe-metallated **MOF-525/PCN-224** phases amongst the three possible Zr_6-TCCP-based MOF products (Fig. 1), the non-metallated products also being synthesized for reference purposes.

In the present work, we thus investigate the immobilization of the PW_{12} POM into Zr_6-TCCP-based MOFs and its impact on the obtained mixture of phases. A structuring effect of the POM is reported towards the targeted kinetic **MOF-525/PCN-224** phases. A complete structural characterization of the product is provided by using Pair Distribution Function (PDF) analysis along with DFT calculations.

The synthesis of the mixed phases **MOF-525/PCN-224**, adapted from reported procedures,[14,19–21] consists of the preparation of Zr_6 clusters in solution at a high temperature followed by the addition of porphyrin and stirring at RT for a week (Fig. 2). We adopted the notation suggested by Gong *et al.*,[14] **Zr_6-TCPP-T** and **Zr_6-TCPP-Fe-T**, where *T* refers to the synthesis temperature. The powder X-ray diffraction (PXRD) diagrams of **Zr_6-TCPP-25** and **Zr_6-TCPP-Fe-25** correspond expectedly to the simulated diagrams of the kinetic phases, **MOF-525** and/or **PCN-224** (Fig. S1a, ESI†). Regarding the immobilization of PW_{12} into the MOFs, the post-synthetic impregnation strategy was discarded, knowing that both **PCN-224** and **MOF-525** exhibit small windows which preclude the diffusion of the POM into the MOF. We thus rather adopted an *in situ* strategy by adding $(TBA)_3PW_{12}O_{40}$ into the synthetic medium. However, RT synthesis failed to incorporate PW_{12} into the MOF. Increasing the synthesis temperature was found to be essential to allow its successful incorporation and obtain the targeted **PW_{12}@Zr_6-TCPP-120** and **PW_{12}@Zr_6-TCPP-Fe-120** after 1 h at 120 °C. For the same experiment at 100 °C and 65 °C, less crystalline phases are obtained (Fig. S2, ESI†). We focused on the impact of a stepwise increase in the amount of PW_{12} introduced into the reaction medium of **PW_{12}@Zr_6-TCPP-Fe-120** on the resulting MOFs' topologies while keeping all the other synthetic parameters constant (Fig. 3). Notably, in the absence of PW_{12} in the reaction medium, the high temperature synthesis of **Zr_6-TCPP-Fe-120** leads to a mixture of the thermodynamic phase, **MOF-545(Fe)**, and of the kinetic ones, **MOF-525(Fe)/PCN-224(Fe)**.

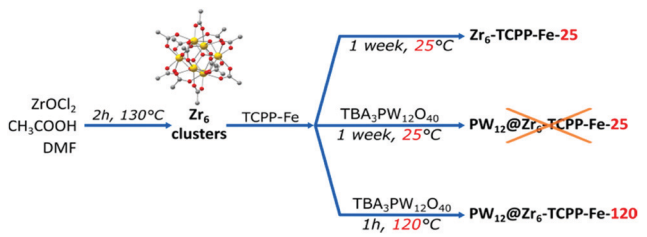

Fig. 2 Synthetic routes adopted for **Zr_6-TCPP-Fe** and **PW_{12}@Zr_6-TCPP-Fe**. The non-metallated compounds are isolated using similar procedures (see ESI†).

This latter result falls in line with the temperature-topology relationship recently reported.[14] Strikingly, the formation of the thermodynamic phase **MOF-545(Fe)** is, however, suppressed upon the addition of a very low amount of PW_{12} (Fig. 3a, red), pointing towards a remarkable structure-directing effect of PW_{12} in the high temperature synthesis. All the PXRD diagrams of the **PW_{12}@Zr_6-TCPP-Fe-120** composites obtained for higher PW_{12} amounts are similar, corresponding to **PCN-224(Fe)** or to the **MOF-525(Fe)/PCN-224(Fe)** mixture.

The IR spectra of this series show the unambiguous presence of the POM within all **PW_{12}@Zr_6-TCPP-Fe-120** materials, exhibiting the characteristic P–O (1077 cm^{-1}), W=O (972 cm^{-1}) and W–O–W (892 and 797 cm^{-1}) vibration bands of PW_{12} (Fig. 3b and Fig. S1b, ESI†). The absence of the aliphatic C–H vibrations in the IR spectra of the composites indicates that no TBA was inserted in the matrix during the synthetic process. A semi-quantitative analysis of the IR spectra was undertaken by following the relative intensities of the bands at 1077 cm^{-1} (noted A), typical of PW_{12}, and at 1180 cm^{-1} attributed to the $\nu_{C-C} + \nu_{C-N}$ vibrations (noted B), typical of the studied MOFs. The evolution of this ratio reveals that a maximum amount of POM immobilized into the MOF is reached for *ca.* 30 mg of $(TBA)_3PW_{12}O_{40}$ in the reaction medium, corresponding to a PW_{12}/Zr molar ratio of 0.05 (Fig. 3c). **PW_{12}@Zr_6-TCPP-120** was also synthesized for further characterization purposes (see Experimental section). The POM loading was evaluated using EDS (Table S1, ESI†), suggesting an average of 1 POM every 2 Zr_6 units in the free-base **PW_{12}@Zr_6-TCPP-120** and 1 POM every 4 Zr_6 units in the Fe-metallated **PW_{12}@Zr_6-TCPP-Fe-120**. C, H, and N analyses indicate missing linkers in both cases, a consequence of the immobilization of the negatively charged POMs and of the presence of the **PCN-224** phase.

In addition, N_2 sorption isotherms (Fig. S3, ESI†) evidence a decrease of the surface area of the POM@MOF compounds when compared to that of the POM-free **Zr_6-TCPP-Fe-25** material, as expected from the incorporation of PW_{12} into the MOF's pores. More importantly, the solid-state NMR $^{31}P\{^1H\}$ CPMAS spectra of **PW_{12}@Zr_6-TCPP-120** and **PW_{12}@Zr_6-TCPP-Fe-120** (Fig. S4, ESI†) clearly show a characteristic single peak at −15.9 ppm and −15.5 ppm, respectively, in the expected chemical shift range for PW_{12},[22] thus suggesting the integrity of the POM. Moreover, the line broadening and appearance of a spinning sideband in the spectrum of **PW_{12}@Zr_6-TCPP-Fe-120** are due to chemical shift anisotropy and anisotropic bulk magnetic susceptibility broadening of ^{31}P nuclei in interaction with the Fe^{III} paramagnetic centre.

In addition, **PW_{12}@Zr_6-TCPP-Fe-120** and **PW_{12}@Zr_6-TCPP-120** were studied using cyclic voltammetry (CV) by the deposition of a thin film of the composites on a glassy carbon electrode (Fig. S5, ESI†). The electrochemical signatures of PW_{12}[24] and TCPP-Fe[12] in solution have been compared to those of the POM@MOF composites, showing that not only were they in full agreement with those reported in the literature but they also allowed the characteristic redox peaks of these two components on the composite materials to be unambiguously attributed. To further investigate the structural features of these porphyrin-based MOFs, a Pair Distribution

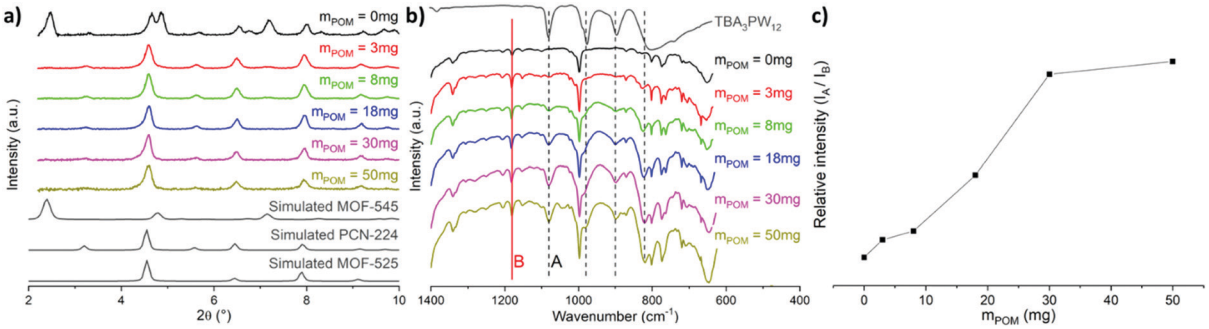

Fig. 3 Impact of a stepwise increase of the amount of PW_{12} in the synthesis medium of **PW_{12}@Zr_6-TCPP-Fe-120** on its (a) PXRD and (b) IR spectra where black dashed lines indicate bands characteristic of PW_{12} while the red line indicates a band of the MOF host. (c) Evolution of the ratio between the intensities of the A and B bands (see text).

Function (PDF) analysis was undertaken. Reflecting the probability of finding two atoms separated by a distance *r*, PDF data provide quantitative information about the local atomic structure, while giving a global overview of the sample. They have proved to be particularly powerful in the field of MOFs recently.[25] In a first step, considering that we may have a mixture of structurally related MOFs, **MOF-525** and/or **PCN-224**, which are difficult to distinguish using PXRD only, we investigated the use of PDF intending to identify the distinctive features related to each phase. This was undertaken using **Zr_6-TCPP-Fe-25** as a case study. As references, the PDF profiles of **MOF-525** and **PCN-224** were simulated using their DFT-optimized crystal structures. They exhibit common features due to their common Zr-oxocluster but also distinctive particularities (see ESI† for details, Fig. S6–S8). The PDF profile of **Zr_6-TCPP-Fe-25** exhibits specific features from both MOFs (Fig. S9, ESI†). On one hand, it has strong similarities with that of **MOF-525**, with a distinct peak at 3.1 Å and a relatively intense peak at 5.1 Å, which are both a signature of Zr-connected TCCP linkers. On the other hand, secondary features suggest the possible presence of **PCN-224** in **Zr_6-TCPP-Fe-25**, such as a rather intense peak at 4.0 Å (associated to –OH and H_2O molecules in place of missing linkers) and a similar PDF profile to that of **PCN-224** in the [5.5–7.5 Å] radial distance range. Overall, this analysis indicates that **Zr_6-TCPP-Fe-25** is unambiguously a mixture of **MOF-525** and **PCN-224**.

In a second step, PDF data were further exploited to investigate the structural integrity of the immobilized POM within **PW_{12}@Zr_6-TCPP-Fe-120**. Using the differential PDF method (d-PDF)[26] recently applied to characterize a POM@UiO-67 composite,[10] the d-PDF of the immobilized PW_{12} was obtained by subtracting directly the PDF of **Zr_6-TCPP-Fe-25** from that of **PW_{12}@Zr_6-TCPP-Fe-120** (Fig. 4a and Fig. S10, see ESI† for details). The POM's d-PDF profile is compared in the 1–10 Å range to that of an isolated $PW_{12}O_{40}^{3-}$ calculated from reported crystallographic data[23] (Fig. 4b). The two PDFs are indeed very similar allowing a precise assignment of all PDF peaks to characteristic W–O and W–W distances and a refinement of the PW_{12} structure as illustrated in Fig. 4c (see ESI† for details, Fig S11 and Table S2). The relatively good quality of the refinement (R_w = 29.3%) and the refined structure of PW_{12} indicate that the POM is indeed fully preserved upon its immobilization in **Zr_6-TCPP-Fe-120**.

To get an in-depth insight into the host–guest interactions at play between the PW_{12} and the MOF, Density Functional Theory (DFT) calculations were performed using **MOF-525(Fe)** phase as the main host. In a first step, simulated annealing (SA) calculations followed by dispersion-corrected DFT-D3 geometry optimizations were done to identify the most likely position of the POM in **MOF-525(Fe)** and qualify its host–guest interactions within the MOF. They reveal a non-centered positioning of the

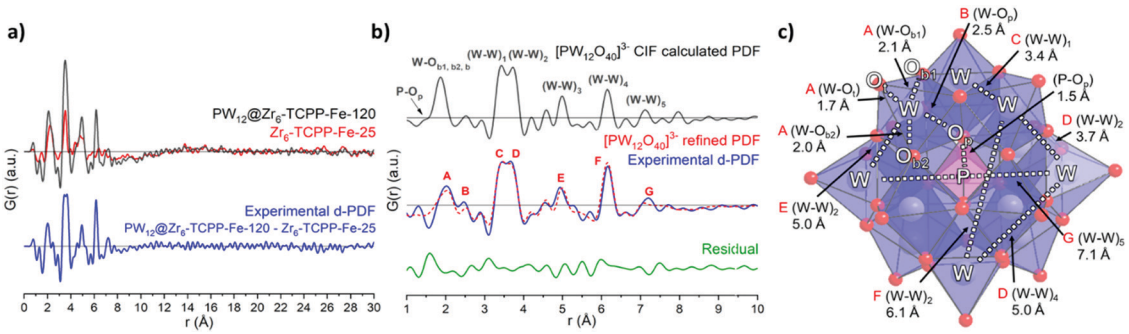

Fig. 4 (a) PDF profiles for **PW_{12}@Zr_6-TCPP-Fe-120**, **Zr_6-TCPP-Fe-25** and the resulting d-PDF associated with the immobilized PW_{12}. (b) Comparison of the calculated PDF of an isolated PW_{12} from reported crystallographic data[23] and the experimental d-PDF associated with PW_{12} in **PW_{12}@Zr_6-TCPP-Fe-120**, superimposed with the refined d-PDF and residual profile. A–H labels of peaks correspond to the indicated refined distances in the POM structure as illustrated in (c). WO_6, blue octahedra; PO_4, pink tetrahedron; O, red sphere; W, grey spheres; P, pink sphere.

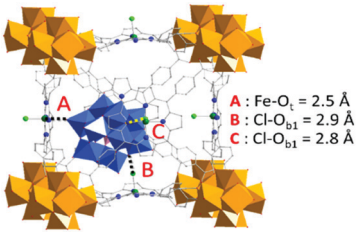

Fig. 5 Most likely positioning of the POM inside the hybrid framework obtained by DFT calculations.

POM within the MOF's cubic cage showing PW_{12} cornered close to a Zr-oxocluster inorganic node (Fig. 5). The interaction energy between PW_{12} and **MOF-525(Fe)** was estimated to be -422 kJ mol^{-1}, which corresponds to coordination-like interactions between the O_{POM} atoms and Fe ions of the TCCP linkers and dispersive interactions with Cl atoms, in addition to POM-TCCP hydrogen bonds (Fig. S12a, ESI†). These results correlate well with the 2D ^{31}P–^{1}H correlation MAS NMR experiment (Fig. S12b, ESI†) demonstrating the spatial proximity of the POMs to the inorganic nodes. Overall, DFT calculations coupled with solid-state NMR added remarkable insights on the POM-MOF interactions to PDF analysis.

In conclusion, with the aim of targeting porphyrinic POM@MOF systems, the addition of the PW_{12} polyoxometalate in the synthetic medium of porphyrin MOFs was explored using a high temperature one-pot synthetic protocol. In the absence of POM, a mixture of the kinetic **MOF-525/PCN-224** and thermodynamic **MOF-545** topologies is obtained. Remarkably, the addition of PW_{12} in the synthetic medium prevents the formation of the expected thermodynamic **MOF-545** phase while favoring the formation of the kinetic ones even at a high temperature, pointing towards the structure-directing role of the POM. Simultaneously we developed in-depth characterization methods for **PW_{12}@MOF** by utilizing the differential Pair Distribution Function as a direct structural signature of the POM, solid-state NMR and DFT calculations. They unequivocally showed the structural integrity of the POM inside the porphyrinic MOF along with an insight into the host–guest interactions between the different components, circumventing the difficulties inherent to the Rietveld refinement of powder X-ray diffraction data of such long-range disordered materials. These results open the way for more complete research on the templating effect of POMs on the topology of porphyrinic MOFs and their effect on their catalytic properties.

This work was supported by CNRS, UVSQ, the Ministère de l'Enseignement Supérieur, de la Recherche et de l'Innovation, the French ANR as part of the 'Investissements d'Avenir' program no. ANR-11-IDEX-0003-02 and CHARMMMAT ANR-11-LABX-0039. This work has been sponsored by the Ile-de-France Region in the framework of Respore, the Île-de-France network of Excellence in Porous Solids. The IMAP laboratory is gratefully acknowledged for N_2 porosimetry measurements. The calculations have been performed using the HPC resources from GENCI (CINES) through Grant A0050907343.

Conflicts of interest

There are no conflicts to declare.

Notes and references

1 A. Bavykina, N. Kolobov, I. S. Khan, J. A. Bau, A. Ramirez and J. Gascon, *Chem. Rev.*, DOI: 10.1021/acs.chemrev.9b00685.
2 P. Horcajada, R. Gref, T. Baati, P. K. Allan, G. Maurin, P. Couvreur, G. Férey, R. E. Morris and C. Serre, *Chem. Rev.*, 2012, **112**, 1232–1268.
3 A. Kirchon, L. Feng, H. F. Drake, E. A. Joseph and H.-C. Zhou, *Chem. Soc. Rev.*, 2018, **47**, 8611–8638.
4 Z.-Y. Gu, J. Park, A. Raiff, Z. Wei and H.-C. Zhou, *ChemCatChem*, 2014, **6**, 67–75.
5 W.-Y. Gao, M. Chrzanowski and S. Ma, *Chem. Soc. Rev.*, 2014, **43**, 5841–5866.
6 W. Morris, B. Volosskiy, S. Demir, F. Gándara, P. L. McGrier, H. Furukawa, D. Cascio, J. F. Stoddart and O. M. Yaghi, *Inorg. Chem.*, 2012, **51**, 6443–6445.
7 D. Feng, W.-C. Chung, Z. Wei, Z.-Y. Gu, H.-L. Jiang, Y.-P. Chen, D. J. Darensbourg and H.-C. Zhou, *J. Am. Chem. Soc.*, 2013, **135**, 17105–17110.
8 J.-S. Qin, S. Yuan, C. Lollar, J. Pang, A. Alsalme and H.-C. Zhou, *Chem. Commun.*, 2018, **54**, 4231–4249.
9 G. Paille, M. Gomez-Mingot, C. Roch-Marchal, B. Lassalle-Kaiser, P. Mialane, M. Fontecave, C. Mellot-Draznieks and A. Dolbecq, *J. Am. Chem. Soc.*, 2018, **140**, 3613–3618.
10 Y. Benseghir, A. Lemarchand, M. Duguet, P. Mialane, M. Gomez-Mingot, C. Roch-Marchal, T. Pino, M.-H. Ha-Thi, M. Haouas, M. Fontecave, A. Dolbecq, C. Sassoye and C. Mellot-Draznieks, *J. Am. Chem. Soc.*, 2020, **142**, 9428–9438.
11 D. Li, M. Kassymova, X. Cai, S.-Q. Zang and H.-L. Jiang, *Coord. Chem. Rev.*, 2020, **412**, 213262.
12 I. Hod, M. D. Sampson, P. Deria, C. P. Kubiak, O. K. Farha and J. T. Hupp, *ACS Catal.*, 2015, **5**, 6302–6309.
13 H. Zhang, J. Wei, J. Dong, G. Liu, L. Shi, P. An, G. Zhao, J. Kong, X. Wang, X. Meng, J. Zhang and J. Ye, *Angew. Chem., Int. Ed.*, 2016, **55**, 14310–14314.
14 X. Gong, H. Noh, N. C. Gianneschi and O. K. Farha, *J. Am. Chem. Soc.*, 2019, **141**, 6146–6151.
15 M. L. Kelty, W. Morris, A. T. Gallagher, J. S. Anderson, K. A. Brown, C. A. Mirkin and T. D. Harris, *Chem. Commun.*, 2016, **52**, 7854–7857.
16 S. M. Shaikh, P. M. Usov, J. Zhu, M. Cai, J. Alatis and A. J. Morris, *Inorg. Chem.*, 2019, **58**, 5145–5153.
17 P. Deria, J. Yu, R. P. Balaraman, J. Mashni and S. N. White, *Chem. Commun.*, 2016, **52**, 13031–13034.
18 P. Deria, D. A. Gómez-Gualdrón, I. Hod, R. Q. Snurr, J. T. Hupp and O. K. Farha, *J. Am. Chem. Soc.*, 2016, **138**, 14449–14457.
19 M. R. DeStefano, T. Islamoglu, S. J. Garibay, J. T. Hupp and O. K. Farha, *Chem. Mater.*, 2018, **30**, 2193–2197.
20 H. Noh, C.-W. Kung, T. Islamoglu, A. W. Peters, Y. Liao, P. Li, S. J. Garibay, X. Zhang, M. R. DeStefano, J. T. Hupp and O. K. Farha, *Chem. Mater.*, 2018, **30**, 2193–2197.
21 G. Kickelbick, P. Wiede and U. Schubert, *Inorganica Chim. Acta*, 1999, **284**, 1–7.
22 W. Salomon, C. Roch-Marchal, P. Mialane, P. Rouschmeyer, C. Serre, M. Haouas, F. Taulelle, S. Yang, L. Ruhlmann and A. Dolbecq, *Chem. Commun.*, 2015, **51**, 2972–2975.
23 A. Kremenović, A. Spasojević-de Biré, R. Dimitrijević, P. Sciau, U. B. Mioč and P. Colomban, *Solid State Ion.*, 2000, **132**, 39–53.
24 K. Eda and T. Osakai, *Inorg. Chem.*, 2015, **54**, 2793–2801.
25 C. Castillo-Blas, J. M. Moreno, I. Romero-Muñiz and A. E. Platero-Prats, *Nanoscale*, DOI: 10.1039/D0NR01673J.
26 K. W. Chapman, P. J. Chupas and C. J. Kepert, *J. Am. Chem. Soc.*, 2005, **127**, 11232–11233.